



HAL
open science

New phenomenological material constitutive models for the description of the Ti6Al4V titanium alloy behavior under static and dynamic loadings

Mariem Yaich, Adinel Gaurus

► **To cite this version:**

Mariem Yaich, Adinel Gaurus. New phenomenological material constitutive models for the description of the Ti6Al4V titanium alloy behavior under static and dynamic loadings. *Procedia Manufacturing*, 2020, *Procedia Manufacturing*, 47, pp.1496-1503. 10.1016/j.promfg.2020.04.336 . hal-02892920

HAL Id: hal-02892920

<https://hal.science/hal-02892920v1>

Submitted on 25 Aug 2020

HAL is a multi-disciplinary open access archive for the deposit and dissemination of scientific research documents, whether they are published or not. The documents may come from teaching and research institutions in France or abroad, or from public or private research centers.

L'archive ouverte pluridisciplinaire **HAL**, est destinée au dépôt et à la diffusion de documents scientifiques de niveau recherche, publiés ou non, émanant des établissements d'enseignement et de recherche français ou étrangers, des laboratoires publics ou privés.



23rd International Conference on Material Forming (ESAFORM 2020)

New Phenomenological Material Constitutive Models for the Description of the Ti6Al4V Titanium Alloy Behavior Under Static and Dynamic Loadings

Mariam YAICH^a, Adinel GAVRUS^{a,*}

^aINSA Rennes, LGCGM - EA 3913, 20 Av. des Butes de Coesmes, F-35708 Rennes, France

* Corresponding author. Tel.: +33-22-323-8666. E-mail address: Adinel.Gavrus@insa-rennes.fr

Abstract

The analysis and optimization of rapid or severe material forming process, where high gradients of plastic deformations, strain rates and temperatures are reached during the material flow, remains today a major challenge. Several light metallic alloys, as the titanium ones, are widely used in many industrial applications. Despite their wide spread adoption, particular phenomena are encountered during their machining: high plastic strains gradients, heavy strain rate localization, chip segmentation, accelerated tool wear, etc. Although the recent advances in the experimental devices, it is still difficult experimentally to investigate the instantaneous mesoscopic phenomena taking place during severe forming processes. Therefore, the use of numerical simulations, in addition to specific experimental measurements, presents an efficient alternative for a better understanding of machining processes. Given thought the significant sensitivity of the modelling to the reliable definition of the thermo-visco-plastic workpiece material behavior and referring to the physically based mesoscopic constitutive model proposed in previous works of Gavrus, this study focuses on formulating and identifying phenomenological rheological laws. Their ability to accurately reproduce the isotropic plastic behavior of the Ti6Al4V titanium alloy for both static and dynamic loadings states, as well as in a wide range of plastic strains, plastic strain rates and temperatures, is checked. A specific iterative non-linear regression method is used for the identification of all corresponding material parameters. Their adequacy is discussed and comparisons with experimental results of the literature are set up. A specific user material subroutine VUHARD© is implemented into the commercial code Abaqus®/Explicit. Numerical simulations of experimental compression tests are performed to valid the rheological models' identification and the material flow prediction. A 2D Finite Element Modelling of the Ti6Al4V orthogonal cutting is performed and the accuracy of proposed constitutive models is examined.

© 2020 The Authors. Published by Elsevier Ltd.

This is an open access article under the CC BY-NC-ND license (<https://creativecommons.org/licenses/by-nc-nd/4.0/>)
Peer-review under responsibility of the scientific committee of the 23rd International Conference on Material Forming.

Keywords: Mesoscopic Constitutive Models; Plastic Behavior; Static & Dynamic Loadings; Strain Rate Effect; Temperature Sensitivity; High Speed Cutting

1. Introduction

The machining of metallic materials, regarded as a rapid material forming process, generally results in specific and severe local thermomechanical deformation phenomena. The workpiece material is subjected to large plastic strains, strong strain-rate gradients, high temperature rise and important nonlinearities. Moreover, severe contact conditions are taking places in very thin material layers. The tool life and the surface quality are consequently influenced. Therefore, the machining process remains problematic for both researchers and industrials, mainly for metals with a relatively poor

machinability like the Ti6Al4V titanium alloy. Despite the interesting mechanical properties of this alloy (low density, high strength at elevated temperature, significant creep property, good corrosion resistance), many problems are involved during its machining due to its low thermal conductivity and high chemical reactivity with the cutting tool materials: chip segmentation even under low cutting conditions, significant fluctuations of the cutting forces, limited tool life, low machined surface quality, etc. Despite the numerous efforts carried out for more control of the Ti6Al4V machining, the use of experimental post-mortem and in-situ observations is still insufficient to well understand the

2351-9789 © 2020 The Authors. Published by Elsevier Ltd.

This is an open access article under the CC BY-NC-ND license (<https://creativecommons.org/licenses/by-nc-nd/4.0/>)
Peer-review under responsibility of the scientific committee of the 23rd International Conference on Material Forming.

10.1016/j.promfg.2020.04.336

local and instantaneous changes followed by the machined material. Therefore, the development of reliable numerical analyses, in addition to experimental observations, is heavily required for a robust control and optimization of machining process. Among the numerical modelling techniques developed during the last decades, the Finite Elements Modelling (FEM) which allows an enhanced understanding of the machining process. It enables a detailed investigation of physical thermomechanical transient phenomena and nonlinearities involved during the chip formation.

However, a well reproduction of the thermomechanical material behavior on both bulk area and machined surface, as well as under severe plastic strains, strain rates and temperatures, is one of the key points to guarantee the highest reliability of a numerical analysis. The definition of constitutive equations able to suitably reproduce the strong coupling between the plastic hardening [1-3] and the softening effects due to severe deformation loadings as the dynamic recovery, recrystallization or phase transformation [4-11], is heavily recommended for an accurate prediction of the machining process, as pointed out in recent works of Gavrus et al. [9], Arrazola et al. [12] and Melkote et al. [13].

In previous scientific works many constitutive laws have been used to model the machining [11-21]. The majority of these laws is based on traditional well-known formulations and can be classified in two main categories: the phenomenological models and the physically based ones. Even though the laws of the second category permit to take into account the microstructure evolution and the deformation history on a mesoscopic scale, they have been uncommonly used to model severe dynamic forming processes and their definition remains today a genuine challenge. On the other hand, the outstanding success of classical empirical models describing the flow stress is mainly due to their relatively simpler and faster parameters' identification. In a classical way, the majority of these laws only takes into account the macroscopic phenomena. They generally reproduce the material sensitivity to the plastic strain, the strain rate and the temperature. A reduced number of material coefficients and weakly coupled or even uncoupled phenomena terms, compared to those of the physically based models, are defined.

The rheological parameters' identification of specific constitutive equations often depends on the local deformation variables and the analytical description of material flow. It is directly carried out based on simpler experimental mechanical tests and on non-linear regression methods used to fit the experimental true stress-true plastic strain curves corresponding to different plastic strain rates and temperatures. Their adequacy in terms of properly modelling the thermomechanical phenomena taking place during a machining process is limited for particular loading conditions. Indeed, their extrapolation is not often allowed. On this point of view, the inverse analysis principle [6], [22-26] based on the minimization of a least-squares function, which is given as the error between the global measurements (forces, torques, specimen shape) and the FEM computed ones, can be used to take into account the whole loadings complexities of a mechanical test, similar to the real ones involved during severe forming processes.

In order to take into account the plastic material strengthening, the strain-rate and the temperature effects during the modelling of the isotropic rheological flow, the empirical work hardening, as those proposed by Hollomon [1], Voce [2] and Ludwik [3], has been defined in previous scientific works of the literature. To take into account the strain rate effect, Norton-Hoff or Zerilli-Armstrong, Cowper-Symonds [4], Johnson-Cook [5], Sokolowski or Sellars-Tegart [27] formulations are generally used. Nonetheless, many laws as Johnson-Cook [5], Zhao-Gary [28], Vinh et al. [29] and Arrhenius [30] ones have been defined to model the material thermal softening effect in the case of numerical studies focusing on the investigation of the thermomechanical coupling. The development of new constitutive models, which accurately take into account the influence of high strain rate gradients, temperature rise and mesoscopic dynamic softening phenomena involved during a plastic deformation, is remaining today a scientific challenge. In this aim, this paper deals with an analytical and numerical analysis of a mesoscopic quasi-static/dynamic behavior of the Ti6Al4V alloy. Starting from the physically based constitutive model proposed by Gavrus [6-9], able to describe the plastic behavior for both low and high strain rates while taking into account important gradients of plastic deformation, strain rate and temperature, different phenomenological models were proposed and analyzed. Experimental compression tests' results of the literature [11] were used and a specific multi-steps non-linear regression method was adopted to identify the coefficients of all studied rheological models. Comparisons between the experimental true stress - true plastic strain flow curves and the computed ones were performed for different strain rates and temperatures. The identified constitutive models were implemented in the FEM code Abaqus®/Explicit via the user-material subroutine VUHARD©. The built-in Johnson-Cook (JC) law, already predefined in Abaqus®, was used to valid the performed programming. Comparisons of numerical results predicted with the developed subroutine and those directly modelled with Abaqus® were done. FEM of compression tests were performed to numerically validate the rheological models and the parameters identification. Finally, numerical simulations of the Ti6Al4V orthogonal dry machining under several cutting conditions were discussed.

Nomenclature

GV	Generalized Voce
CS	Cowper-Symonds
JC	Johnson-Cook
ASH	Arc Sinus Hyperbolic
RJC	Regularized Johnson-Cook
GJC	Generalized Johnson-Cook
ALE	Arbitrary Eulerian Lagrangian
LAG	Lagrangian

2. Mesoscopic phenomenological constitutive equations

This study proposes an investigation of the isotropic thermo-visco-plastic behavior of the Ti6Al4V alloy. The dynamic work hardening, the material sensitivity to the strain

rate and the thermal softening effects were investigated. Based on previous research works of Gavrus [6-9], where the kinetics of dislocations slips due to plastic deformations and thermal activation energy governing microscopic evolution phenomena (as hardening, dynamic recovery, recrystallization phase transformation and twinning) have been taken into account, the isotropic equivalent von Mises stress $\bar{\sigma}$ can be expressed as a function of the true plastic strain ε , the true plastic strain rate $\dot{\varepsilon}$ and the temperature T as follow:

$$\bar{\sigma} = \sigma_e(\dot{\varepsilon}, T) + \sigma_y(\varepsilon, \dot{\varepsilon}, T) \tag{1}$$

where $\sigma_e(\dot{\varepsilon}, T)$ is the initial elastic limit and $\sigma_y(\varepsilon, \dot{\varepsilon}, T)$ is the yield stress, given respectively by the following equations:

$$\sigma_e(\dot{\varepsilon}, T) = \sigma_0 \times G(\dot{\varepsilon}) \times F(T) \tag{2}$$

$$\sigma_y(\varepsilon, \dot{\varepsilon}, T) = [H(\varepsilon) \times (1 - W) + W \times \sigma_s] \times G(\dot{\varepsilon}) \times F(T) \tag{3}$$

Here σ_0 is the elastic yield stress for a reference value of strain rate and temperature. $H(\varepsilon)$, $G(\dot{\varepsilon})$ and $F(T)$ are respectively the hardening, the strain rate sensitivity and the thermal softening functions. W is the material fraction undergoing dynamic softening phenomena (dynamic recrystallization, phase transformation, twinning) described by the Avrami expression $W = 1 - \exp(-R \times \varepsilon^s)$ where R and S are the softening variables and σ_s is the saturation flow stress. Consequently, $\bar{\sigma}$ can be written in the following form:

$$\bar{\sigma} = [\sigma_0 + H(\varepsilon) \times (1 - W) + W \times \sigma_s] \times G(\dot{\varepsilon}) \times F(T) \tag{4}$$

As shown by S. Liu et al. [10], the hardening term corresponding to biphasic materials can be expressed by:

$$H(\varepsilon) = H_\alpha(\varepsilon) \times \varphi + H_\beta(\varepsilon) \times (1 - \varphi) \tag{5}$$

Here $H_\alpha(\varepsilon)$ and $H_\beta(\varepsilon)$ represent the hardening terms of the α and the β phases respectively, while the fraction of the principal phase is defined by $\varphi \in [0, 1]$. Referring to Rotella et al. [31], only a low percentage of the β phase is available in the Ti6Al4V (about 10%-20%). This justifies the assumption made in this study regarding a homogeneous microstructure of the α - β Ti6Al4V titanium alloy. Hence, the same material hardening function was defined to predict the effect of the plastic strain ($H(\varepsilon) = H_\alpha(\varepsilon) = H_\beta(\varepsilon)$). For the common empirical models of the literature, the hardening isotropic material has been predicted through a Ludwik power law [3]:

$$H_{LDK}(\varepsilon) = B \times \varepsilon^n \tag{6}$$

where B and n are the hardening coefficients.

The hardening term can be considered as a result of a threshold flow stress once a critical plastic strain is reached. Consequently the observed dynamic recovery phenomenon characterizing large plastic deformations of Ti6Al4V alloy requires to take into account the effect of the progressive

reduction of the material strengthening in the flow stress evolution. Therefore, the generalized Voce hardening model [2], [6-8] (GV), given by Eq. (7), was chosen in this study.

$$H_{GV}(\varepsilon) = B \times [1 - \exp(-n \times \varepsilon)]^{n_a} \tag{7}$$

where B , n , n_a are the hardening coefficients of the GV law.

According to recent scientific works [7-8], n_a has specific values (0.5 for FCC metals, 1 for CC ones and 2 for HC ones).

The prediction of the material sensitivity to the strain rate was carried out using specific terms (see Eqs (8-11)) as Cowper-Symonds (CS), Johnson-Cook (JC), regularized Johnson-Cook (RJC) and particularly Arc Sinus Hyperbolic (ASH) law as proposed by Gavrus in previous works [7-10].

$$G_{CS}(\dot{\varepsilon}) = 1 + 0.5 \times \left(\frac{\dot{\varepsilon}}{\dot{\varepsilon}_0} \right)^C \tag{8}$$

$$G_{JC}(\dot{\varepsilon}) = \begin{cases} 1 & (\text{if } \dot{\varepsilon} < \dot{\varepsilon}_0) \\ 1 + C \times \ln\left(\frac{\dot{\varepsilon}}{\dot{\varepsilon}_0}\right) & (\text{if } \dot{\varepsilon} \geq \dot{\varepsilon}_0) \end{cases} \tag{9}$$

$$G_{RJC}(\dot{\varepsilon}) = 1 + C \times \ln\left(1 + \frac{\dot{\varepsilon}}{\dot{\varepsilon}_0}\right) \tag{10}$$

$$G_{ASH}(\dot{\varepsilon}) = 1 + ASH \left[0.5 \times \left(\frac{\dot{\varepsilon}}{\dot{\varepsilon}_0} \right)^C \right] \tag{11}$$

For all these strain-rate functions, C is the strain rate sensitivity coefficient and $\dot{\varepsilon}_0$ is the reference strain rate characterizing the transition between the static and the dynamic states. It is noted that the JC model is applied for strain rates higher than the reference one $\dot{\varepsilon}_0$. In order to avoid the numerical problems due to its extrapolation for strain rates lower than $\dot{\varepsilon}_0$, the discontinuous regularization method adopted by the FEM code Abaqus® was firstly used. Because of possible significant local gradients of the strain rate leading to a discontinuous evolution mainly for $\dot{\varepsilon} < \dot{\varepsilon}_0$, a continuous regularization of the JC strain rate sensitivity term was adopted. The definition of the ASH term (Eq (11)) in this study aimed to take into account the important gradients of strain rates, where both quasi-static and dynamic loadings (low and high strain rates respectively) are involved as in the case of localized shear bands. The ASH function is given by the inverse of the sinus hyperbolic:

$$ASH(x) = Sinh^{-1}(x) = \ln\left(x + \sqrt{1 + x^2}\right) \tag{12}$$

It can be proven that Eq. (11) is close to a CS power law for small strain rates and a JC logarithmic one for high values.

Regarding the thermal softening effect, many scientific works of the literature were focused on accurately predicting the material sensitivity to the temperature. Due to the limits of the JC law [5], mainly due to its constant thermal softening coefficient m , many modifications have been proposed [10],

[15], [20-21], [31]. In this study, two temperature sensitivity terms were defined and compared: the standard JC one (Eq. 13) and that proposed by S. Liu et al. [10] (Eq. 14).

$$F_{JC}(T) = 1 - \left(\frac{T - T_R}{T_M - T_R} \right)^m \quad \text{if } T_R \leq T < T_M \quad (13)$$

$$F_{GJC}(T) = \left[1 - k \times \left(\frac{T - T_R}{T_M - T_R} \right)^m \right]^j \quad \text{if } T_R \leq T < T_R + (T_M - T_R) \left(\frac{1}{k} \right)^{\frac{1}{m}} \quad (14)$$

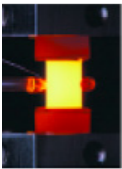
where m, j and k are the temperature sensitivity coefficients. T is the material temperature, T_R is the reference temperature (293 K) and T_M is the material melting temperature (1943 K).

As shown in Eq. (14), the thermal sensitivity term GJC is a generalized form of the JC law ($k = j = 1$). Therefore, its definition aimed to overcome, through the additional coefficients j and k , the limits of the JC law due to its single constant coefficient m , and thereby to reproduce the observed sigmoidal form of the material thermal softening. However, the possible material softening caused by a dynamic recrystallization and phase transformations, due to the plastic deformation, was neglected in this study i.e. $R = S = 0$. According to above constitutive models (Eq. (4), Eq. (7-11) and Eq. (13-14)), a total of eight phenomenological models, corresponding to all combinations of the proposed plastic strain, strain rate and temperature sensitivity terms were investigated. Their identifications were performed using a specific multi-steps non-linear regression method.

3. Constitutive coefficients identification

Experimental compression tests of the literature [11], performed with a Gleeble machine on cylindrical Ti6Al4V specimens ($H_0/D_0 = 1.5$) at different constant crushing speeds ($V = V_0 = \text{cte}$) and initial temperatures T_0 , were used for the identification of all previous phenomenological models. The experimental loading conditions are summarized in Table 1.

Table 1. Experimental compression loadings ($D_0 = 6.65$ mm, $H_0 = 9.95$ mm).

Operating Variable	Compression speed ($V=V_0$) (mm/s)	Initial temperature T_0 (K)	
	0.1	293	
		473	
		673	
		873	
		1073	
	1000	0.1	293
		1	
		10	
		100	
		1000	

The influence of the machine rigidity and the offset of the loads applied to the specimen were taken into account to improve the force-displacement curves recordings. Even though a low friction has been induced in the specimen-tool interfaces during the compression tests, resulting in a weak

heterogeneity of the plastic flow, the raw experimental data were used to compute analytically the true stress-true plastic strain flow. A hypothesis of homogeneous deformation has been used. Numerical FEM simulations were then performed to verify the analytically computed local plastic flow stress.

A specific multi-steps parameters' identification procedure, based on a non-linear regression method, was used to determine the coefficients values of all studied phenomenological models. The optimal parameters guess of the $P_G = \{\sigma_0, B, n, n_a, C, \dot{\epsilon}_0, m, j, k\}$ vector were determined for every rheological law by minimizing, in a least squares sense, the error between the experimental true stress-true plastic strain curves and the computed ones for each iterative updated parameters set. The general error function given in previous research works [6], [24] was defined by:

$$Q = \sum_{i=1}^{n_i} \gamma_i \times \left[(\bar{\sigma}(P))_i - (\sigma_{\text{exp}})_i \right]^2, \quad \gamma_i = 1 / \sum_{i=1}^{n_i} \left[(\sigma_{\text{exp}})_i \right]^2 \quad (15)$$

where n_i is the total number of experimental measurements corresponding to investigated loading conditions. σ_c and σ_{exp} are respectively the computed and the experimental flow stresses. γ_i is the weighting or scaling factor equal here to the inverse of the quadratic norm of experimental data.

For all studied rheological models, the same initial parameters values of P_G^0 were defined in order to separately investigate the effect of each chosen phenomenological law on the accurate prediction of the material behavior for different loadings. A specific non-linear iterative strategy was adopted. It is based on the following steps:

- Identification of the hardening and the viscosity coefficients B, n and C .
- Identification of the thermal softening coefficient m .
- Identification of the initial yield stress σ_0 .
- Identification of the reference strain rate $\dot{\epsilon}_0$.
- Identification of the GV hardening exponent n_a .
- Identification of the GJC exponent j .
- Identification of the GJC coefficient k .

The main purpose of this multi-steps identification procedure was to allow a successive reduction of the cost function error while guaranteeing physically based constitutive coefficients values. To avoid the local minimums, the coefficients identified after each step were considered as intermediate ones to obtain high accuracy of the parameters estimation. They were re-computed during the non-linear regression procedure. The two last steps were skipped for the JC thermal softening term.

The identification results of rheological models composed of the GV hardening law, the CS, JC, RJC or ASH strain rate sensitivity term and the GJC thermal softening term are grouped in Table 2. The errors between the experimental and the analytically computed true stress-true plastic strain curves obtained after every identification step and corresponding to all investigated strain rate sensitivity functions G are illustrated in Fig. 1. A pronounced reduction of identification errors was underlined in the 2nd, the 6th and in the 7th steps, where the thermal softening parameters m, j and k was done

respectively. Even though these almost similar errors, an increase of the model reliability was noted for the ASH law.

Table 2. Constitutive coefficients identified for different strain rate sensitivity terms G where $\bar{\sigma} = (\sigma_0 + H_{(GV)}) \times G \times F_{(GJC)}$ and $W = 0$ ($R = S = 0$) in Eq. (4).

Variable	Initial parameters	Identified parameters			
		$\bar{G}_{(CS)}$	$\bar{G}_{(JC)}$	$\bar{G}_{(RJC)}$	$\bar{G}_{(ASH)}$
σ_0 (MPa)	944	611.62	946.85	914.37	613.35
B (MPa)	500	206.76	331.95	308.59	209.02
n	0.5	17.44	14.63	19.95	17.67
n_a	1	0.75	0.73	0.79	0.81
C	0.1	0.012	0.012	0.015	0.008
$\dot{\epsilon}_0$ (s^{-1})	1	2.35	1.1	1.41	1.98
m	1	1.99	1.96	1.91	1.97
k	1	1.12	1.11	1.11	1.12
j	1	5.37	5.16	5.29	5.25
Error Q _(Step1) (%)	–	44.19	30.12	26.04	43.96
Error Q _(Step7) (%)	–	6.8	6.85	7.1	6.54

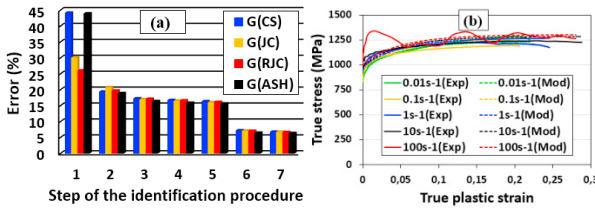


Fig. 1. (a) Least-squares errors Q of stresses for different identification steps and strain rate sensitivity functions (293K) and (b) comparison of the experimental and the computed true stress-true plastic strain curves for different initial strain rates ($293K_ \sigma_{Mod} = H_{GV}(\dot{\epsilon}) \times G_{ASH}(\dot{\epsilon}) \times F_{GJC}(T)$).

Figure 2 illustrates a comparison between all investigated strain rate and thermal softening sensitivity functions.

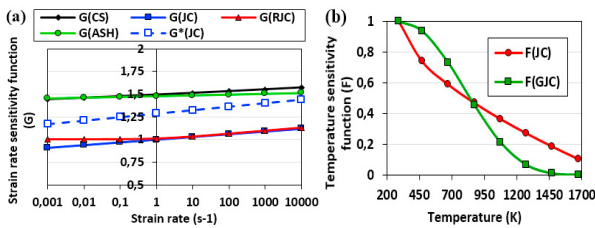


Fig. 2. Sensitivity terms variation: (a) of the material viscosity $G(\dot{\epsilon})$ using $F_{GJC}(T)$ and (b) of the thermal softening $F(T)$ using $G_{ASH}(\dot{\epsilon})$.

For low strain rates, high correlation levels between the G functions corresponding to the CS and the ASH laws were reached for initial strain rates below $1 s^{-1}$. However, the mismatch was increased for the highest strain rate, in the case of the CS function. Contrariwise, important disagreement between the ASH and the JC laws was underlined, even for high strain rates. It is justified by the significant mismatch noted between the identified initial yield stresses σ_0 . A new $G^*(JC)$ function, corresponding to the $G_{(JC)}$ one and multiplied by the ratio $\sigma_{0(JC)}/\sigma_{0(ASH)}$, was plotted. It resulted in more agreement with $G_{(ASH)}$ especially for high strain rates. This

justifies the ability of the ASH law to accurately reproduce both low and high strain rates as has been proved by Gavrus [7-9]. Therefore, the advantageous of the ASH law in terms of accurately predicting the material strain rate sensitivity, mainly the transition between the lowest and the highest values, was underlined. Contrariwise, the performed comparisons confirmed the limits related to the extrapolation of the CS (or the JC) law for high (or low) strain rates, where a non-physical prediction of the specimens' material behavior was encountered. For the thermal softening prediction, Fig. 2b underlines the inadequacy of the JC term, which leads to a quasi-linear evolution of the F function, totally unlike the GJC term resulting in a sigmoidal variation. Therefore, the definition of the GJC allowed more reliable prediction of the temperature effect on the Ti6Al4V material behavior, thus more significant correlations between the experimental and the analytically computed stress-plastic strain curves (Fig. 3b). However, in the case of the JC thermal softening function (Fig. 3a), only the experimental results at particular initial temperatures (e.g. 293K and 873K) were suitably reproduced, underlining the inadequacy of the classical JC law in terms of well reproducing the Ti6Al4V sensitivity to the temperature.

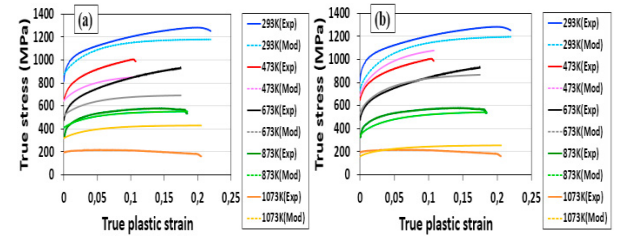


Fig. 3. Comparison of the experimental and the computed true stress-true plastic strain curves corresponding to different temperatures and thermal softening functions (initial strain rate of $0.01 s^{-1}$): (a) F_{JC} and (b) F_{GJC} .

Regarding the prediction of the coupled effects of the plastic strain, plastic strain rate and temperature, the most reliable phenomenological law can be written in this form:

$$\sigma = \left(\sigma_0 + B \times \left[1 - \exp(-n \times \epsilon) \right]^n \right) \times \left(1 + ASH \left[0.5 \times \left(\frac{\dot{\epsilon}}{\dot{\epsilon}_0} \right)^c \right] \right) \times \left[1 - k \times \left(\frac{T - T_R}{T_M - T_R} \right)^m \right] \text{ if } T_R \leq T < T_R + (T_M - T_R) \left(\frac{1}{k} \right)^{\frac{1}{m}} \quad (16)$$

4. Numerical validation

Numerical axisymmetric simulations of Ti6Al4V compression tests were performed using the commercial code Abaqus®/Explicit. The same loading conditions and initial cylindrical specimens' geometry as the experimental ones were defined (see Table 1). Adiabatic conditions were assumed using a Taylor-Quinney factor of 0.9. The investigated phenomenological models were numerically implemented into the user VUHARD© subroutine. Different contact conditions of specimen-tool plate interfaces: frictionless, moderate friction and sticking were simulated to

investigate the friction effect on the modelling reliability. In the case of a moderate friction, a Coulomb-Tresca law was defined ($\mu = 0.21$, $\bar{m}_{Tresca} = 1$ and $\tau_{lim} = \sigma_{av} / \sqrt{3} = 421MPa$, where σ_{av} is the average flow stress estimated for the equivalent plastic deformation energy balance computed from the reference hardening curve corresponding to $0.01 s^{-1}$, 293 K and a true plastic strain below 0.2). A quadrilateral axisymmetric FE mesh with a reduced integration degree and a deformation-temperature coupling (CAX4RT) was used. Rigid bodies were defined to model the tool plates. The built-in JC phenomenological model [9] predefined in the FEM code Abaqus® was adopted for the VUHARD© validation. High agreements were noted between the numerical results directly computed with Abaqus® and those modelled with the developed user subroutine. Afterword, comparisons between the FEM numerical force-displacement curves and the experimental ones were set up. The case of a JC thermal softening term was firstly considered to investigate separately the effect of strain rate sensitivity functions. Fig. 4 illustrates the computed errors in terms of the axial forces and true stresses predicted with different contact conditions.

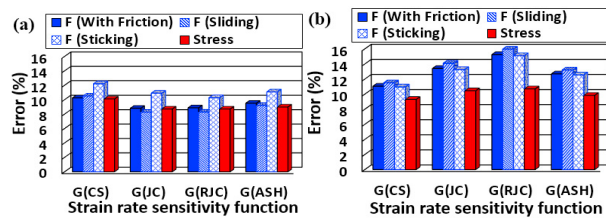


Fig. 4. Errors of FEM upsetting forces F (in blue) and flow stresses (in red) computed for different friction conditions, strain rate sensitivity models, initial strain rates and 1.5 mm crushing (293K): (a) $100 s^{-1}$ and (b) $0.01 s^{-1}$.

Similar errors' trends for both numerical forces and flow stresses were underlined for all investigated contact conditions. The use of JC and RJC strain rate sensitivity terms gives lowest mismatches with the experimental results for an initial strain rate of $100 s^{-1}$, while more important differences were observed for a strain rate of $0.01 s^{-1}$. These results justify their adequacy only for high strain rates, totally unlike the CS law giving good agreements with experimental observations only for low strain rates. Nonetheless, the prediction of low and high strain rate effects was simultaneously enabled with the ASH law. It led to more accurate predictions, mainly when it is coupled with the GJC thermal softening model. This highlighted the effect of both strain rate and temperature sensitivity laws on the FEM reliability. A low sensitivity of the numerical results to the contact conditions was also pointed out. For same compression loadings ($0.01 s^{-1}$, 293K), low disagreements between the numerical forces were observed underlining the weak effect of friction. However, slight mismatched deformation modes and flow stress distributions were noted for all investigated contact conditions (Fig. 5). Concerning the numerical upsetting loads, a relatively weak sensitivity to friction conditions was pointed out. It underlined the accuracy of the homogeneity assumption set up to compute analytically the true stress-true plastic strain curves, directly used by the non-linear regression method.

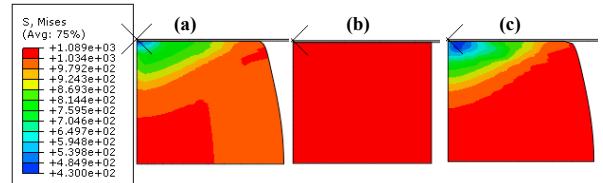


Fig. 5. Cylindrical deformed specimens' shapes corresponding to a FEM crushing of 1.5 mm for three contact conditions ($0.01 s^{-1}$, 293K, $\sigma = H_{Gv}(\epsilon) \times G_{ASH}(\dot{\epsilon}) \times F_{JC}(T)$): (a) moderate friction, (b) sliding and (c) sticking conditions.

This low friction effect on the flow stress values and specimen shape is due to the chosen slender cylindrical specimen ($H_0/D_0 = 1.5$) and to the maximum reached plastic strain (below 0.3). The stress heterogeneity was more accentuated for the sticking contact, where no sliding occurred at the specimen-tool interfaces. Furthermore a slightly bulging cylinder was observed in the case of a moderate friction.

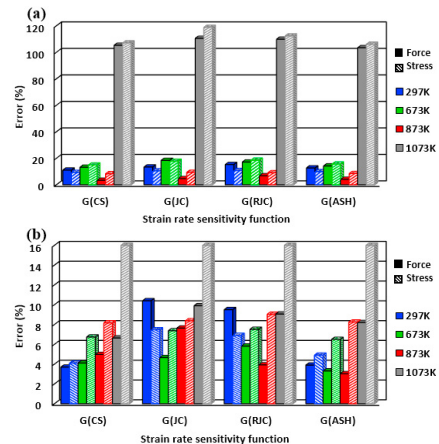


Fig. 6. Comparisons of computed FEM forces and flow stresses errors corresponding to a 1.5 mm crushing and a $0.01 s^{-1}$ strain rate for different initial temperatures and thermal softening functions: (a) $F_{(JC)}$ and (b) $F_{(GJC)}$.

The accuracy of all performed identifications was also checked for four initial temperatures: 293K, 673K, 873 and 1073K. For an initial strain rate of $0.01 s^{-1}$, the FEM of the compression tests gives correlated forces and flow stresses errors (Fig. 6). Concerning the JC thermal softening term reliability, significant mismatch with the experimental loads and flow stresses were underlined when an initial temperature of 1073K was defined. For a lower temperature of 673 K, mismatched results were also predicted. However, the rheological law based on the GJC term allowed a reliable prediction of the Ti6Al4V behavior at different temperatures, mainly when it was coupled with the ASH strain rate sensitivity term (Fig. 6b).

It should be noted that even though accurate predictions were obtained with the adopted non-linear identification, rigorous predictions of the material behavior can be obtained by an inverse analysis based on minimizing the error between the experimental and the computed FEM loads, as well as the specimen shape [22-26].

5. High speed machining modelling

5.1 Numerical orthogonal cutting model

In order to evaluate the robustness of the proposed phenomenological models, 2D numerical simulations of the Ti6Al4V orthogonal dry machining at room temperature were performed using the Abaqus®/Explicit code. Linear quadrilateral FE mesh, with a reduced integration and coupled deformation-temperature conditions (CPE4RT) were used. A tungsten carbide cutting tool was considered as a rigid body characterized by an edge radius of 20 μm, a clearance equal to 2° and rake angles of 7°. The model geometry, the mesh and the boundary conditions defining the mesoscopic area of the orthogonal dry finishing cutting are pictured in Fig. 7.

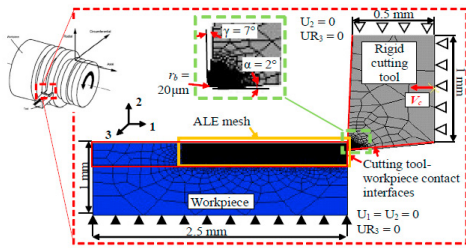


Fig. 7. Orthogonal cutting model, geometry/mesh and boundary conditions.

The case of an orthogonal finishing cutting process was investigated. A feed rate of 0.1 mm/rev, a depth of cut of 3 mm and two cutting speeds of 60 m/min and 180 m/min were considered. Both Lagrangian (LAG) and Arbitrary Eulerian Lagrangian (ALE) formulations were used. The remeshing was only applied to a small part of the workpiece (the chip part, the cutting tool passage zone and the machined surface), subjected to severe local loadings during the cutting process (see Fig. 7). Whereas, a LAG mesh was defined to the rest of the model geometry. The discretization of the workpiece upper part, where the ALE formulation was defined, and of the cutting tool edge radius, was done with a refined mesh to well reproduce the geometry changes as well as the particularity of the tool shape. This meshing strategy aimed to reduce the computing time, significantly increased by the ALE formulation and the mesh refinement. To predict the thermo-visco-plastic workpiece material flow, the phenomenological models with (a) an isotropic recovery hardening term of GV, (b) a strain rate sensitivity term of CS, RJC or ASH and (c) a thermal softening term of GJC were chosen. The coefficients of all investigated rheological models are grouped in Table 2. A Coulomb-Tresca friction law was used to predict the sticking-sliding in the cutting tool-workpiece interfaces. The influence of dissipated energy by plastic deformation and friction on the temperature rise was taken into account. For this study the material damage behavior was not considered.

5.2 Results and discussion

Figure 8 illustrates the numerical chip shape and the computed cutting and feed forces corresponding to the three rheological models, for a cutting distance of 0.9 mm.

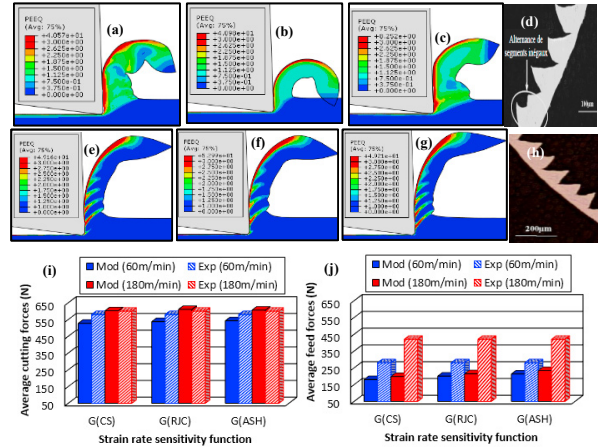


Fig. 8. Effects of strain rate sensitivity terms G and of cutting speed on the FEM chip morphology and the average predicted forces: (a) G(CS)_60 m/min, (b) G(RJC)_60 m/min, (c) G(ASH)_60 m/min, (d) exp_60 m/min [32], (e) G(CS)_180 m/min, (f) G(JCR)_180 m/min, (g) G(ASH)_180 m/min); (h) exp_180 m/min [33], (i) cutting forces and (j) feed forces.

Different chip morphologies were predicted, depending on the defined rheological model. For a cutting speed of 60 m/min, slight chip segmentation was noted in the case of the CS and of the ASH strain rate sensitivity terms. Contrariwise, totally continuous chip was predicted with the RJC law. With the increase of the cutting speed, more localized adiabatic shear bands were modelled with all compared laws, especially for ASH formulation. Distinct numerical forces F_c and F_f were computed along the cutting and feed directions respectively for a 3 mm width. The lower values were predicted with the CS strain rate sensitivity term, while the highest ones were modelled using the ASH law (Fig. 8i and Fig. 8j). Referring to the experimental results of Calamaz [32], the material flow stress given by Eq. (16), using the ASH term, lead to the most reliable numerical results. Moreover the most pronounced chip's deformation localizations, in agreement with the experimental morphology, were predicted with this law. Furthermore, the corresponding FEM average cutting and feed forces are in good agreement with the experimental ones, pointing out the accuracy of the ASH strain rate sensitivity model. However, the low local outbreak chip's geometry instabilities corresponding to a weak chip segmentation is due, as highlighted by Yaich et al. [33], to the major influence of the adaptive remeshing procedure.

6. Conclusion

The adequacy of different mesoscopic phenomenological models in terms of accurately predicting the thermo-viscoplastic material behavior of Ti6Al4V was analyzed. A general Voce term (GV) was used in order to reproduce the work hardening of the biphasic titanium alloy, as well as the dynamic recovery due to its micro-structure change during a plastic deformation. The analysis of the material sensitivity to the strain rate and to the temperature based on the definition of different constitutive equations' terms was performed. The identification of all studied rheological models was carried out

for both quasi-static and high strain rates, as well as for different initial temperatures. The comparisons between four strain rates sensitivity laws (CS, JC, RJC and ASH laws) underlined the limited suitability of the power CS and the logarithmic JC models for particular strain rate range. The adequacy of the CS model was highlighted only for lowest strain rates, while the material behavior under high strain rates was adequately modelled with a JC or a RJC form. Contrariwise, the ASH law showed an interesting ability to accurately predict all investigated strain rates ranges. In terms of suitably predicting the temperature effects on the Ti6Al4V alloy behavior, the definition of two temperature sensitivity terms, the JC and the GJC ones, highlighted the inadequacy of the JC law and the accuracy of the GJC one. A phenomenological model based on a GV hardening term, an ASH strain rate sensitivity function and a GJC thermal softening term was proposed. The efficiency of the multi-steps non-linear identification procedure was also proved through the numerical validations performed by FEM simulations of studied experimental compression tests. The good agreements obtained between the experimental, numerical and the analytically computed results underlined the robustness of both identifications and numerical implementations. Finally, the performed 2D FEMs of the Ti6Al4V orthogonal dry cutting process at a mesoscopic scale highlighted the significant sensitivity of chip segmentation to the strain rate term. Despite the advantage related to the ALE formulation, mainly summarized on the authorized nodes relocation according to the material deformation, a reliable prediction of chip segmentation was allowed using ASH law. A better description of the strain rate gradients on the adiabatic shear bands and of the plastic strain localizations was observed.

Acknowledgements

This scientific work is funded by the University of Brittany Loire (France) and the French Brittany Region under the Res. Post-Doc Contract 1-2018-SAD-USIAERO 2019-2020.

References

- [1] Hollomon J. H. Tensile deformation. *Trans. ASME* 1945; 162268–290.
- [2] E. Voce. The relationship between stress and strain for homogeneous deformations. *J. Inst. Met.* 1948; 74:537–562.
- [3] Ludwik P.. *Element der technologischen. Mechanik* 1909; 32.
- [4] Cowper P.S., Symonds G. R.. Strain hardening and strain rate effects in the impact loading of cantilever beams. 1957.
- [5] Johnson G. R., Cook W. H. . A constitutive model and data for metals subjected to large strains, high strain rates and high temperatures. *Proc. of the 7th Int. Symp. on Ballistics* 1983; 547: 541–547.
- [6] Gavrus A. Automatic Identification of Rheological Parameters by Inverse Analysis. PhD Thesis. Ecole Nat. Sup. des Mines, Paris. 1996.
- [7] Gavrus A.. Formulation of a new constitutive equation available simultaneously for static and dynamic loadings. *EDP Sci. Web of Conf. Proc. DYMAT* 2009. p. 1239–1244.
- [8] Gavrus A. Constitutive Equation for Description of Metallic Materials Behavior during Static and Dynamic Loadings Taking into Account Important Gradients of Plastic Deformation. *Key Eng. Mater.* 2012; 504–506: 697–702.
- [9] Gavrus A., Caestecker P., Ragneau E. Finite Element Analysis of the Influence of the Material Constitutive Law Formulation on the Chip Formation Process. *ASME Proc. of 11th Int. Conf. ESDA*; 2012
- [10] Liu S., Kouadri-Henni A., Gavrus A. DP600 dual phase steel thermo-elasto-plastic constitutive model considering strain rate and temperature influence on FEM residual stress analysis of laser welding. *J. Manuf. Process.* 2018 ; 35 :407–419.
- [11] Braham-Bouchnak T. Etude du comportement en sollicitations extrêmes et de l'usinabilité d'un nouvel alliage de titane aéronautique: le Ti555-3. PhD Thesis. Ecole Nat. Sup. d'Arts et Métiers, Angers. 2010.
- [12] Arrazola P. J., Özel T., Umbrello D., Davies M., Jawahir I. S. Recent advances in modelling of metal machining processes. *CIRP Ann. Manuf. Tech.* 2013; 62(2): 695–718.
- [13] Melkote S. N. et al. Advances in material and friction data for modelling of metal machining, *CIRP Ann.-Manuf. Tech.* 2017; 66(2):731–754.
- [14] Hor A. Simulation physique des conditions thermiques de forgeage et d'usinage-Characterisation et modélisation de la rhéologie et de l'endommagement. PhD Thesis, ENSAM. 2011.
- [15] Sima M., Özel T. Modified material constitutive models for serrated chip formation simulations and experimental validation in machining of titanium alloy Ti6Al4V. *J. Mech. Tools Manuf.* 2010; 50(11): 943–960.
- [16] Follansbee P. S., Kocks U. F. A constitutive description of the deformation of copper based on the use of the mechanical threshold stress as an internal state variable. *Acta Metall.* 1988; 36(1): 81–93.
- [17] Fergani O., Atmani Z., Zenasni M., Sorby K.. Physics-based Model to Predict Forces and Chip Morphology in the Machining of a Ti6-Al-4V Alloys for Aeronautical Applications. *Procedia Manuf.* 2016; 6: 53–62.
- [18] Hijaz H., Zain-ul-Abdein M., Saleem W., Asad M., Mabrouki T. Numerical simulation of the effects of elastic anisotropy and grain size upon the machining of AA2024. *Mech. Sci. Technol.* 2018; 344:522-542.
- [19] Calamaz M., Coupard D., Girod F. A new material model for 2D numerical simulation of serrated chip formation when machining titanium alloy Ti-6Al-4V. *Int. J. Mach. Tools Manuf.* 2008; 48(3–4): 275–288.
- [20] Hor A., Morel F., Lebrun J. L., Germain G. Modelling, identification and application of phenomenological constitutive laws over a large strain rate and temperature range. *Mech. Mater.* 2013; 64 : 91–110.
- [21] Yaich M. Contribution à la fiabilisation de la modélisation numérique de l'usinage de pièces en titane. PhD Thesis, ENI Sfax/ENSAM. 2017.
- [22] Lovato G., Moret F., Cailletaud G., Pilvin P. Identification of viscoplastic constitutive equations by inverse method. *Comp. Mech.* 1995.
- [23] Gelin J. C., Ghouati O. The inverse approach for the determination of constitutive equations in metal forming. *CIRP Ann. Manuf. Technol.* 1995; 44(1): 189–192.
- [24] Gavrus A., Massoni E., Chenot J. L. The analysis of inelastic behavior formulated as an inverse rheological approach. *Meas. Sci. Technol.* 1998; 9: 848-863.
- [25] Fourment L., Vieilledent D. Shape optimization for metal forging problems: Determination of an objective function for flow defects. *European Congress ECCOMAS*. 2000. p. 1–18.
- [26] Gavrus A., Davoodi B., Ragneau E.. A study of material constitutive behavior at elevated temperature from compressive SHPB test using an inverse analysis method. *J. Phys. IV.* 2006; 134: 661–666.
- [27] Sellars C. M., Tegart W. J. Relationship between strength and structure in deformation at elevated temperatures. *Mem.Sci.Rev.Mettal.* 1966; 63(731–745).
- [28] Zhao G., Gary H. The testing and behavior modelling of sheet metals at strain rate from 10^{-4} to 10^5 s⁻¹. *Mater. Sci. Eng.* 1996; 207(1): 46–50.
- [29] Vinh A., Afzali T., Roche M. Mechanical behavior of materials. K.J. Miller, R.F. Smith. Press, Oxford - New York, 1980.
- [30] Samantaray A. K., Mandal D., Bhaduri S.. Constitutive analysis to predict high-temperature flow stress in modified 9Cr-1Mo steel. *Mater. Des.* 2010; 31(2): 981–984.
- [31] Rotella G., Dillon J. O., Umbrello D., Settineri L., Jawahir I. S. The effects of cooling conditions on surface integrity in machining of Ti6Al4V alloy. *Int. J. Adv. Manuf. Tech.* 2014 ; 71(1–4) : 47–55.
- [32] Calamaz M. Approche expérimentale et numérique de l'usinage à sec de l'alliage aéronautique TA6V. PhD Thesis. Univ. Bordeaux 1. 2008.
- [33] Yaich M., Ayed Y., Bouaziz Z., Germain G. Numerical analysis of constitutive coefficients effects on FE simulation of the 2D orthogonal cutting process: application to the Ti6Al4V. *Int. J. Adv. Manuf. Technol.* 2017; 93(1–4): 283–303.